Research Article Vol. 34, No. 10 / October 2017 / Journal of the Optical Society of America B 2147

Journal of the Optical Society of America B

OPTICAL PHYSICS

Numerical analysis of tip-localized surface plasmon resonances in periodic arrays of gold nanowires with triangular cross section

Ricardo Tellez-Limon,[1,*] Mickaël Février,[2] Aniello Apuzzo,[3] Rafael Salas-Montiel,[4] and Sylvain Blaize[4]

[1]CONACYT - Unidad Monterrey, Centro de Investigación Científica y de Educación Superior de Ensenada, Alianza Centro 504 PIIT, Apodaca, NL 66629, Mexico
[2]E.I. CESI, Campus Ile-de-France/Centre, 93 Bld de la Seine, BP 602, 92006 Nanterre Cedex, France
[3]OLSA S.p.A., R&D Lighting Group, C.so Allamano, 70, 10098 Rivoli (TO), Italy
[4]Laboratoire de Nanotechnologie et d'Instrumentation Optique, Institut Charles Delaunay, CNRS UMR 6281, Université de Technologie de Troyes, 12 rue Marie Curie, CS 42060, 10004 Troyes, France
*Corresponding author: rtellez@conacyt.mx

Received 14 June 2017; revised 4 August 2017; accepted 20 August 2017; posted 21 August 2017 (Doc. ID 297858); published 20 September 2017

In this contribution, we numerically study the tip enhancement of localized surface plasmons in periodic arrays of gold nanowires with triangular cross section under different illumination configurations. We found that the plasmonic resonance in a single nanowire is excited with a transverse magnetic (TM) plane wave impinging from the substrate at the critical angle, whereas grazing angles are required for the excitation of resonant propagating modes in periodic arrays of triangular-shaped nanowires. Moreover, we found that resonant plasmonic quasi-Bloch modes are efficiently excited with the fundamental TM mode of a dielectric waveguide placed underneath the array. The integrated plasmonic structure allows a strong enhancement of the electromagnetic field at the tip of the nanowires, hence its potential application in the development of new nanophotonic devices.

OCIS codes: (130.3120) Integrated optics devices; (250.5403) Plasmonics; (310.6628) Subwavelength structures, nanostructures; (240.6680) Surface plasmons; (230.7370) Waveguides; (160.4236) Nanomaterials.

https://doi.org/10.1364/JOSAB.34.002147

1. INTRODUCTION

Among the large variety of shapes in nanoparticles or cross sections in nanowires, sharp geometries such as nanotips stimulate a great interest in applications where strong light–matter interaction in subwavelength volumes is required [1]. Such nanotips present an extraordinary enhancement of the electromagnetic field relative to the electromagnetic incident field in the vicinity of their apex. In metallic nanoparticles and nanowires, this enhancement is caused by the excitation of localized surface plasmon resonances (LSPRs) polarized along their tip axis [2]. Furthermore, the spectral line shape, amplitude, and width of the LSPR can be tuned by modifying the aspect ratio [3] and radius of curvature [4] of the nanotips, as well as the refractive index of the surrounding medium [5].

This high tunable range in the LSPR of metallic nanocones has been studied for different applications. For example, in a series of works, Fleischer and coauthors demonstrated the enhancement of the electromagnetic field at the tip of arrays of metallic nanocones under illumination with an electric field parallel to the axis of the tip [6]. Moreover, a collective enhancement of the electromagnetic field was measured for an array of nanocones with a subwavelength-scale period [7]. These periodic arrays of nanocones were implemented in microfluidic channels to trap molecules to measure their enhanced fluorescence [8]. Also, Rao and coauthors used metallic nanocones to enhance the Raman signal [9]. In nonlinear optics applications, Bautista and collaborators generated second- and third-harmonic signals in an array of metallic nanocones under proper polarized illumination [10,11]. In solar cells applications, the enhancement of light extraction efficiency using dense arrays of metallic nanocones has been reported [12]. Recent examples for the controlled fabrication of metallic nanocones have been reported in the literature, with technologies such as nanotransfer printing [13] or nanoimprint lithography [14], shadow mask evaporation [7], and ion milling on patterned metallic layers [6]. With this encouraging evolution of the fabrication techniques, the theoretical and numerical analysis of LSPRs under standard experimental conditions becomes a relevant subject.

Among the methods used to perform these analyses in single and in arrays of nanocones, we can find the finite-difference time-domain (FDTD) method, the finite element method [6,15], and the discrete dipole approximation [4].

Periodic arrays of metallic nanowires with triangular cross sections have received less attention than periodic arrays of metallic nanocones in spite of their comparable optical characteristics. As demonstrated by Saison-Francioso *et al.*, due to their bulk refractive index sensitivity—defined as the change in the resonance wavelength of metallic nanowires relative to the variation in the refractive index of the surrounding environment—periodic arrays of nanowires with different cross sections can be applied for biochemical sensing devices [16]. For instance, gold-coated arrays of nanowires with triangular cross section were used for the detection of DNA sequence of molecules by enhancing the surface-enhanced Raman scattering signal [17]. Also, sensors based on one-dimensional periodic arrays of metallic nanowires with trapezoidal cross sections have been investigated in the diffractive regime [18]. Although a strong localization and enhancement of the electromagnetic field near the above-mentioned metallic nanostructures was demonstrated, the illumination of the arrays under transverse magnetic (TM)-polarized light at normal angle of incidence limits their performance because the LSPR along the tip axis of the nanowires is not efficiently excited.

Due to the lack of analysis regarding the way these resonances take place, in this contribution we study the optical properties of periodic arrays of metallic nanowires with triangular cross sections under typical experimental configurations beyond illumination at normal incidence. Furthermore, we analyze the optical response of the periodic arrays in diffractive and sub-diffractive regimes. To this purpose, we use the Fourier modal method (FMM) to calculate the absorption efficiency of an infinite linear array of metallic nanowires with triangular cross section as a function of its period, and as a function of the wavelength and incidence angle of light [Fig. 1(a)]. As we will demonstrate, a dipolar transverse mode (DTM) enhances the electromagnetic field around the tip of the triangular-shaped nanowires. This mode is efficiently excited with TM-polarized light impinging from the substrate at grazing angles. The results imply the use of photonic modes of dielectric waveguides for the excitation of the tip-LSPR [Fig. 1(b)]. We then calculate the dispersion curves of such an integrated system, and plot the transmission, reflection, and extinction spectra under guided wave excitation. Finally, we extend this analysis of triangular-shaped nanowires to three-dimensional nanocones integrated on top of a dielectric waveguide [Fig. 1(c)] thanks to numerical simulations performed with the FDTD method.

2. PLANE-WAVE EXCITATION

The structure consists of an infinite periodic array of gold nanowires with triangular cross section (isosceles triangles of height $h = 144$ nm and width $w = 72$ nm), invariant along the y direction, finite along the z direction, and periodic along the x-axis (Fig. 1). These values are close to reported fabrication parameters [6,14]. The array with period Λ is placed on top of a semi-infinite silica substrate with a constant index of refraction

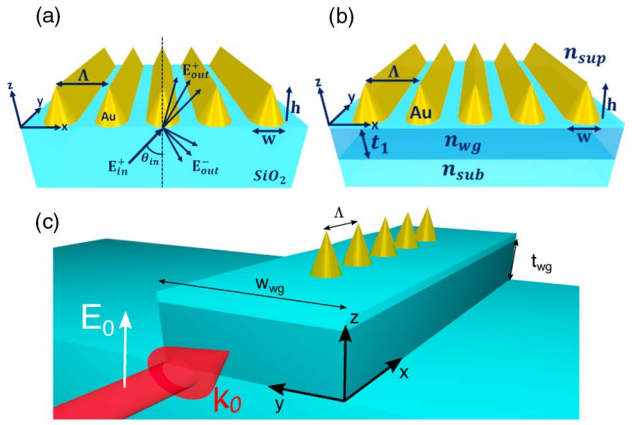

Fig. 1. (a) Schematic representation of the periodic array of gold nanowires with triangular cross section of width $w = 72$ nm, height $h = 144$ nm, and period Λ, on top of a silica substrate. The structure is invariant along the y direction. The incident TM-polarized plane wave forms an angle θ_i relative to the normal. The resulting transmission and reflection are the sum of all diffracted modes, E^{+}_{out} and E^{-}_{out}, in the reciprocal Fourier domain. (b) Schematic representation of the same gold nanowires integrated on top of a dielectric waveguide inside the glass substrate to be analyzed in Section 3. (c) Schematic of a three-dimensional integrated array of gold nanocones placed on top of a dielectric waveguide to be presented in Section 4.

$n_{\text{sub}} = 1.5$. The data of Palik [19] were used for the relative permittivity of gold. The structure is illuminated with a plane wave impinging from the substrate with an incidence angle θ_i measured with respect to the normal. Due to the invariant geometry of the system, we only consider TM-polarized light ($E_y = H_x = H_z = 0$) in order to excite the LSP resonances of the nanowires.

The diffraction of an incident plane wave, with parallel wave vector component β_i, by a periodic array of period Λ, is described by the well-known Bragg formula [20]:

$$\beta_d - \beta_i = \frac{2\pi m}{\Lambda}, \tag{1}$$

where β_d is the parallel wave vector component of the m-th diffracted order ($m \in Z$). Then, the Bragg formula allows determination of the minimum period for a given wavelength that leads to the propagation of diffracted orders either in the substrate or in the superstrate, as

$$\begin{cases} \frac{\lambda}{\Lambda} = \frac{n_{\text{sub}}}{m}\left(\frac{n_i}{n_{\text{sub}}}\sin\theta_i + 1\right), & \text{into the substrate,} \\ \frac{\lambda}{\Lambda} = \frac{1}{m}(n_i \sin\theta_i + 1), & \text{into the superstrate,} \end{cases} \tag{2}$$

where n_i is the refractive index of the incident medium and θ_i is the angle of incidence.

A. Diffractive Regime

Clearly, the diffractive regime allows the existence of at least one diffracted order, and thus λ/Λ verifies one or both of these inequalities:

$$\begin{cases} \frac{\lambda}{\Lambda} \le \frac{n_{\text{sub}}}{m}\left(\frac{n_i}{n_{\text{sub}}}\sin\theta_i + 1\right), & \text{into the substrate,} \\ \frac{\lambda}{\Lambda} \le \frac{1}{m}(n_i \sin\theta_i + 1), & \text{into the superstrate.} \end{cases} \quad (3)$$

Then, to analyze the LSPRs for the structure under study in the diffractive regime, we chose arbitrarily a period of $\Lambda = 6$ μm, which is far above the conditions of Eq. (3) in the visible range.

The plot in Fig. 2(a) shows the absorption spectra as a function of the angle of incidence of light, normalized to an infinite incident plane wave. All spectra were computed with the FMM method (see Methods). These absorption spectra reveal the excitation of a surface plasmon resonance (LSPR) that takes place around $\lambda = 540$ nm. This LSPR reaches a maximum when the illumination is set at the critical angle defined by $\theta_c = \arctan(1/n_{\text{sub}})$. Under illumination at normal incidence, a parallel (longitudinal) dipolar momentum is clearly induced in the nanowire, as shown in the near-field map in Fig. 2(b). As a result two hot spots appear at the lower vertices of the cross section of the nanowire.

At the critical angle ($\theta_c = 41.8°$), a vertical (transverse) effective dipolar momentum appears in the nanowire and excites the tip-LSPR, as it is revealed in Fig. 2(c). More precisely, the field line distribution at the maximum of absorption ($\lambda = 540$ nm, $\theta_c = 41.8°$), identified by the marker R0 in Fig. 2(a), shows that the LSPR at these illumination conditions is a mixture of a transverse and a longitudinal dipolar momentums.

The strong absorption of light at the total internal reflection regime is the result of the surface propagation of the evanescent electromagnetic field with an elliptical polarization state [21,22]. Near to the critical angle, the elliptical polarization state is predominantly linear, with the major axis perpendicular to the air–silica interface, creating a vertical effective dipolar momentum in the nanowire [23]. Furthermore, the polarization ellipticity varies rapidly (as $1/\sin\theta_i$), for θ_i close to $\pi/2$ rad. This rapid variation implies that the wave impinging the surface at an infinite distance from the scatterer, will be coupled into a lateral wave traveling parallel to the surface. Reciprocally, the radiation pattern of a perpendicularly oriented dipole in the superstrate (i.e., in the air) close to the air–silica interface is predominantly directed toward the substrate in the direction of the critical angle θ_c [22]. This means that light impinging from the substrate near to this angle efficiently excites the perpendicular-oriented dipole, and hence the interaction with the nanostructure is improved.

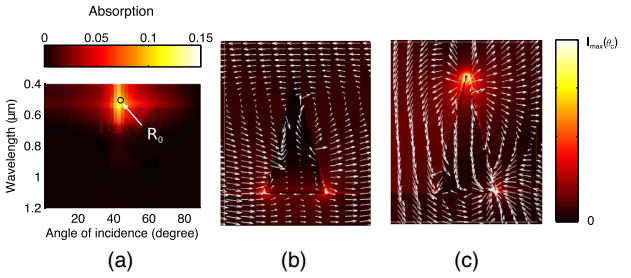

Fig. 2. Illumination of an array of gold nanowires with period $\Lambda = 6$ μm placed on top of a silica substrate with a TM plane wave from the substrate. (a) The absorption as a function of the incidence angle and wavelength is maximum around $\lambda = 540$ nm and $\theta_i = 43°$ (marker R0), near to the critical angle (θ_c). (b),(c) Energy density maps and electric field line distribution under illumination at $\lambda = 540$ nm and at $\theta = 0°$ and $\theta_c = 41.8°$, respectively. The near-field maps were normalized to the maximum intensity of resonance at θ_c and used the same scale bar for comparison only.

B. Sub-Diffractive Regime

The sub-diffractive regime is obtained from Eq. (3) with $m = 1$ and $n_i = n_{\text{sub}}$ as follows:

$$\frac{\lambda}{\Lambda} > (n_i \sin\theta_i + n_{\text{sub}}). \quad (4)$$

For decreasing period, the interaction of the electromagnetic fields between subsequent nanowires evolves from weak far-field coupling to strong near-field coupling including evanescent waves. This change in the nature of the interaction mechanism strongly affects the spectral response of the array. In particular, the LSPR can excite collective Bloch modes [24] that are able to propagate along the array at a grazing angle defined by the zero order of diffraction (i.e., along the x-axis).

First, we consider the variation of the spectral response of the periodic array as a function of the angle of incidence of the TM-polarized plane wave, for a period of $\Lambda = 200$ nm. The width and height of the nanowires remain the same.

Unlike the diffractive regime, the absorption spectra [Fig. 3(a)] exhibit a more complex structure. A LSP resonance is still excited around $\lambda = 530$ nm, near to the value observed for the array of long period. The absorption increases up to 95% at the critical angle (marker R0) and also along the solid blue line between labels R0 and R1 that represents the Bragg condition [Eq. (2)]. This enhancement of the absorption in the array of metallic nanowires is similar to observations made with corrugated metallic gratings. It is known in the literature as the Wood's dispersion anomalies [25], which were interpreted by Fano [26]. In addition, a new resonance is observed at grazing angles with maximum absorption of 87% around $\lambda = 800$ nm [marker R2 in Fig. 3(a)].

To go further in the analysis, we present the absorption spectra as a function of the period in Figs. 3(b)–3(d). The angle of incidence for the TM-polarized plane wave is fixed to $\theta_i = 0°$, $\theta_i = \theta_c$, and $\theta_i = 82°$. The blue and red solid lines represent the cutoff conditions of the subsequent Bragg orders propagating into the silica substrate and air superstrate, respectively (subsequent Brillouin zones). The cutoff wavelength of the m-th Bragg order is given by Eq. (2).

We observe again the excitation of the longitudinal LSPR around $\lambda = 540$ nm both at normal incidence and at the critical angle. Figure 3(c) confirms again a huge increase in the absorption of up to 90% at the critical angle. Remarkably, a strong distortion of the absorption band appears in Fig. 3(c) at the critical angle, for very short periods. This is the result of a strong near-field coupling between the nanostructures. For the grazing angle [Fig. 3(d)], the two LSPRs already observed in Fig. 3(a) (markers R1 and R2) reappear in the first Brillouin zone (sub-diffractive regime) in the absorption spectra. The strong distortion of the bands close to the edge of the first Brillouin zone denotes again a Wood anomaly effect, characterized by an enhancement of the absorption along with a strong redshift of the resonant wavelength. The band containing R1 exhibits

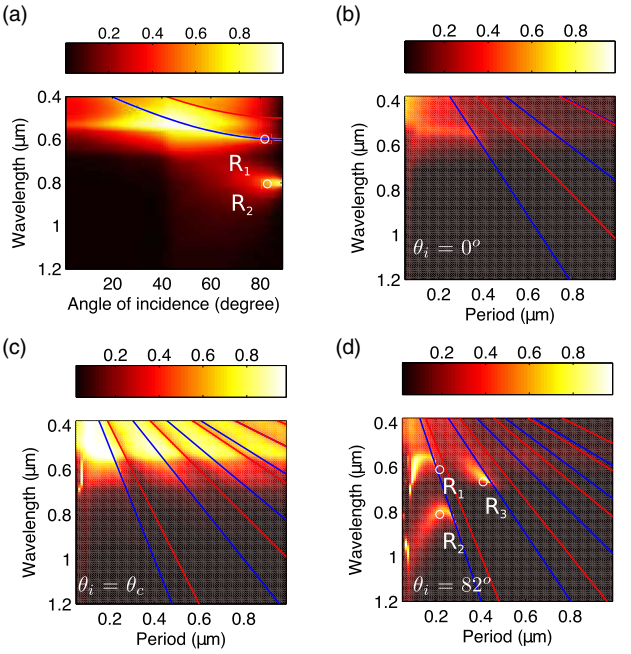

Fig. 3. Normalized absorption efficiency spectra for an infinite periodic array of gold triangular-shaped nanowires illuminated from the substrate with a TM-polarized plane wave. (a) Spectra as a function of the angle of incidence θ_i and period fixed to $\Lambda = 200$ nm. A LSP resonance is excited around $\lambda = 530$ nm, near to the value observed for the array of long period. This resonance is enhanced along the first Bragg order (blue curve) between markers R0 and R1 and at the critical angle (R0). A second resonance is excited at grazing angles with maximum absorption around $\lambda = 800$ nm (R2). Spectra as a function of the period Λ for illumination at (b) normal incidence ($\theta_i = 0°$), (c) at the critical angle ($\theta_i = 41.8°$), and (d) $\theta_i = 82°$. For the latter, the two LSPR [Fig. 3(a)] reappear in the first Brillouin zone (sub-diffractive regime). Close to the edge of the first Brillouin zone is observed a Wood anomaly effect, characterized by an enhancement of the absorption along with a strong redshift of the resonant wavelength. In the second Brillouin zone, only a diffractive dipolar transverse mode (R3) is observed. The blue and red curves represent the wavelength cutoff conditions of the subsequent Bragg orders propagating into the silica substrate and air superstrate, respectively [Eq. (2)].

maxima of absorption of more than 90%, for instance 99.3% of absorption around $\lambda = 600$ nm and a period $\Lambda = 90$ nm, and between 92% and 96% for a period close to $\Lambda = 200$ nm. At the second band containing R2, the absorption has values around 85% at around $\lambda = 750$ nm and $\Lambda = 220$ nm. In the second Brillouin zone (diffractive regime), we found another maximum of absorption of 65% close to edge of the second Brillouin zone around $\lambda = 635$ nm and $\Lambda = 420$ nm [marker R3 in Fig. 3(d)].

To determine the nature of these three resonances, we calculated the near-field distribution of the electromagnetic energy density at the position of tags R1, R2, and R3 in Fig. 4(b). The markers R1 and R2 are the same as those in Fig. 3(d).

The resonance at the position R1 at $\lambda = 600$ nm and $\Lambda = 200$ nm envolve the excitation of a dipolar longitudinal mode (DLM), leading to an enhancement of the electromagnetic energy density at the lower vertices of the triangles [Fig. 4(a)]. A strong enhancement of the optical field at the top vertices

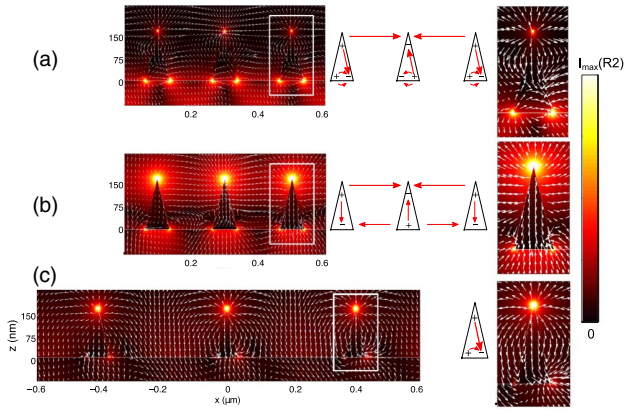

Fig. 4. Energy density maps and electric field line distribution for the chain of nanowires at R1, R2, and R3 illuminated from the substrate with a TM-polarized plane wave at a grazing angle $\theta_i = 82°$. (a) At R1 ($\lambda = 600$ nm and $\Lambda = 200$ nm) the optical field is enhanced at the lower apexes of the nanowires due to the main excitation of the dipolar longitudinal mode. (b) At R2 ($\lambda = 800$ nm and $\Lambda = 200$ nm) the field is strongly enhanced at the top apexes of the nanowires due to a dipolar transverse mode coupling. (c) At R3 ($\lambda = 660$ nm and $\Lambda = 400$ nm) the dipolar transverse coupling is weaker but still observable. The near-field maps were normalized to the maximum intensity of resonance R2 and used the same scale bar for comparison only.

of the triangles is observed in the near-field map at marker R2, located at $\lambda = 800$ nm and $\Lambda = 200$ nm [Fig. 4(b)]. From our numerical results, the enhancement factor of the absolute value of amplitude of the electric field 10 nm above the apex of the nanowires is about 4 times higher relative to the amplitude of the incident electric field. The distribution of the electric field lines reveals the coupling between consecutive nanostructures due to a dipolar transverse resonance. This electric field enhancement was not observed in the diffractive regime, and can be interpreted as a quasi-Bloch mode supported by the periodic array when illuminated with a TM-polarized plane wave at grazing angles [24].

The third resonance, R3, located at a wavelength $\lambda = 660$ nm and a period $\lambda = 400$ nm is due to the propagation of a diffractive dipolar transverse resonance [Fig. 4(c)]. In this case, all the transverse dipoles have the same orientation with a phase difference of 2π rad, instead of the phase difference of π rad observed for the resonance R2 in Fig. 4(b). For R3, we also observe a deformation of the electric field lines at the base of the nanowires caused by the weaker near-field interaction of the dipolar longitudinal mode.

These results demonstrate that the tip-localized LSPR is considerably enhanced by specific conditions of illumination at grazing angles and total internal reflection. Moreover, this field enhancement is solely achievable if the period of the array is short enough to allow the near-field interaction between the nanowires in a sub-diffractive regime.

3. GUIDED-WAVE EXCITATION: TOWARD AN INTEGRATED DEVICE

So far, we presented the optical properties of the nanowire array above the light-line. The transverse dipolar LSPR is responsible

for the enhancement of the tip-LSPR and can be considerably enhanced at grazing illumination angles when the period of the array is small enough. In this section, we further investigate the properties of the nanowire array under the light-line by considering the coupling of the structure with a dielectric waveguide. The dispersion curves of the nanowire array [Fig. 5(a)] along with the dispersion relation of a bare dielectric waveguide [Fig. 5(b)] are depicted in Fig. 5(c). The dielectric waveguide consists of a core of thickness $t_1 = 200$ nm and a refractive index $n_{wg} = 2$ (Si_3N_4 for instance). The core is immersed into the substrate at a distance $t_2 = 30$ nm from the air–silica interface. The thickness of the waveguide was calculated to support the propagation of the fundamental TM0 mode in the spectral range from 500 nm to 1200 nm.

The dispersion curves shown in Fig. 5(c) were computed with the FMM within the first Brillouin zone (first Bragg order) [24]. The colored region corresponds to the normalized absorption efficiency spectra [Fig. 3(a)] and mapped into k_x units through the relationship $k_x = k_0 n_{\text{sub}} \sin\theta_{\text{inc}}\Lambda/\pi$, with $k_0 = 2\pi/\lambda$. The white, black, and green curves represent the light-lines of the air superstrate, silica substrate, and core of the waveguide, respectively. The curve of blue triangles corresponds to the TM0 fundamental mode supported by the isolated dielectric waveguide. As the LSPRs at the position of markers R1 and R2 (Fig. 3) were excited under illumination from the substrate, they are radiated modes appearing above the light-line of the substrate.

The array of nanowires supports two bands of modes [Fig. 5(c)]. The first one is associated with a DLM, which is barely excited near to the Bragg condition (edge of the first zone of Brillouin). Since this band lies above the light-line of the substrate, these are radiated modes, exhibiting an enhancement of the electric field in the bottom apexes of the nanowires [Figs. 5(d) and 5(e)]. The second resonance band [green stars in Fig. 5(c)] is associated with a DTM. Since this mode lies below the light-line of the substrate, it is a guided mode and, therefore, the periodic array of gold nanowires behaves as a plasmonic waveguide. For this quasi-Bloch mode, the electric field is enhanced at the upper apexes of the nanowires [Figs. 5(f) and 5(g)].

We also observe that the DTM crosses the fundamental TM0 mode supported by the dielectric waveguide, at a wavelength value $\lambda = 747$ nm ($k_x = 0.86\pi/\Lambda$). This crossing point indicates that the photonic mode (TM0) can be efficiently coupled to the plasmonic mode (DTM) of the periodic array of gold nanowires as both wavelength and k-vector matches [24].

We then proceed to study the case of the integrated plasmonic structure depicted in Fig. 6(a), consisting of the periodic array of triangular-shaped nanowires placed on top of the dielectric waveguide. In Fig. 6(b) we present the dispersion curves

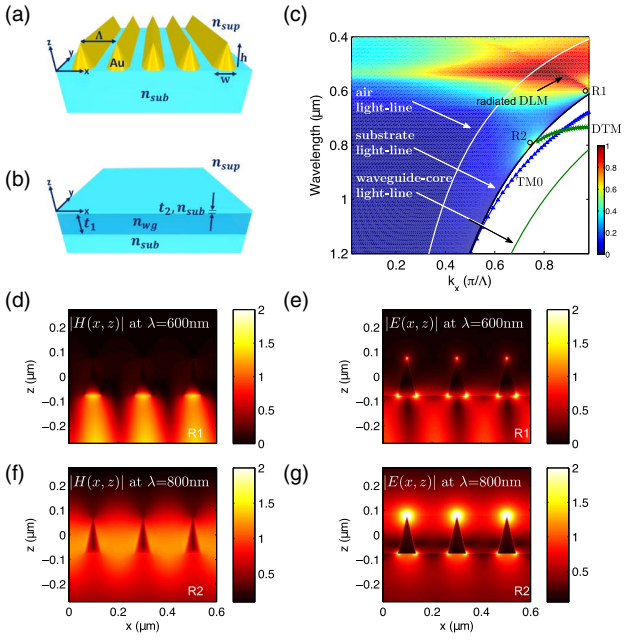

Fig. 5. Schematic representation of (a) an infinite periodic array of gold nanowires with triangular cross section ($w = 72$ nm, $h = 144$ nm, and $\Lambda = 200$ nm) on top of a glass substrate and (b) of an optical planar waveguide (dielectric core of thickness $t_1 = 200$ nm and refractive index $n_{wg} = 2.0$ immersed in a silica substrate $n_{\text{sub}} = 1.5$). The core was separated from the silica–air interface a distance $t_2 = 30$ nm. (c) The dispersion curves show the dipolar transverse mode (DTM) band of the nanowires crossing the fundamental TM0 mode band of the dielectric waveguide around $\lambda = 747$ nm ($k_x = 0.86\pi/\Lambda$). An efficient mode coupling is thus expected at this crossing point for an array placed on top of the waveguide. The dipolar longitudinal modes (DLMs) are radiated modes as they lay above the substrate light-line. Distribution of (d) the magnetic and (e) the electric fields of the dipolar longitudinal eigenmode (DLM) at R1. Distribution of (f) the magnetic and (g) the electric fields of the dipolar transversal eigenmode (DTM) at R2.

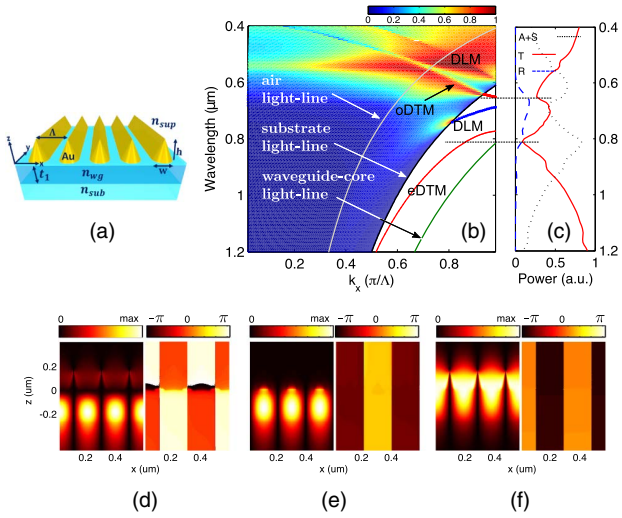

Fig. 6. (a) Representation of a periodic array of 5 Au nanowires on a dielectric waveguide. (b) Dispersion curves of an infinite array of Au nanowires on a dielectric waveguide. The coupled waveguides support an even (eDTM) and an odd (oDTM) dipolar transverse mode. The DLM becomes a guided mode due to the presence of the waveguide. (c) Normalized transmission (red solid line), reflection (blue dashed line), and extinction (black dotted line) spectra of a finite array of five nanowires. The transmission exhibits two minima values around 650 nm and 810 nm. The first corresponds to the excitation of both the DLM and oDTM, while the second of the eDTM. Distribution of the magnitude and phase of the magnetic fields of the (d) oDTM, (e) DLM, and (f) eDTM eigenmodes at the edge of the first Brillouin zone.

of the complete integrated system. Two splitting bands are created around the anti-crossing point ($\lambda = 747$ nm, $k_x = 0.86\pi/\Lambda$). The upper band (red bold curve), namely the odd dipolar transverse mode (oDTM), presents an electromagnetic field that is positive in the nanowires and negative in the waveguide [Fig. 6(d)]. The lower band (red curve) corresponds to an even dipolar transverse mode (eDTM) because the field is positive in both nanowires and the dielectric waveguide [Fig. 6(f)]. This mode splitting confirms the coupling between the DTM and TM0 modes of the isolated structures. We also observe that the initially radiated DLM band (Figs. 3 and 5) becomes a guided mode because its effective index is redshifted due to the presence of the dielectric waveguide. The magnitude and phase of the magnetic near-field maps in Figs. 6(d)–6(f), which allowed us to identify the parity of these modes, were calculated at the edge of the first Brillouin zone.

To corroborate the coupling between the photonic and plasmonic modes, we simulated the beam propagation along the integrated structure with the aperiodic Fourier modal method [24,27,28]. For this simulation, we used a finite number of nanowires (five nanowires), and we launched the fundamental TM0 mode from the input of the dielectric waveguide at $x = 0$. With this implementation, we calculated the transmission, reflection, and extinction (absorption plus scattering) spectra, normalized to the input power [Fig. 6(c)].

The transmission spectrum [red curve in Fig. 6(c)] shows a first minimum value around $\lambda = 650$ nm, which corresponds to the excitation of both DLM and oDTM modes. This situation is corroborated in the magnetic and electric near-field maps of Figs. 7(a) and 7(b), where the electromagnetic field is mainly enhanced at the bottom apexes of the nanowires, as we observed for the plane-wave excitation [Fig. 4(a)].

The efficient excitation of the tip-LSPR is clearly observed in the magnetic and electric near-field maps of Figs. 7(c) and 7(d), at a wavelength value $\lambda = 810$ nm, matching with the second minimum value observed in the transmission spectrum of Fig. 6(c). This tip-LSPR is the result of the efficient excitation of the plasmonic DTM via the fundamental TM0 photonic mode. Moreover, this mode is a propagative mode, because the slope of the dispersion curve for the eDTM is not zero at this wavelength value. According to our numerical results, for this particular wavelength is obtained an enhancement factor of the amplitude of the electromagnetic field of 8.7 times, measured 10 nm above the apex of the nanowire and relative to the amplitude of the incident electromagnetic field.

These results demonstrate that a periodic array of gold nanowires with triangular cross section supports the propagation of a plasmonic mode that can be efficiently coupled to the photonic mode of a dielectric waveguide placed in close proximity to the periodic array. In addition, an efficient excitation of the tip-LSPR of the nanowires is achieved.

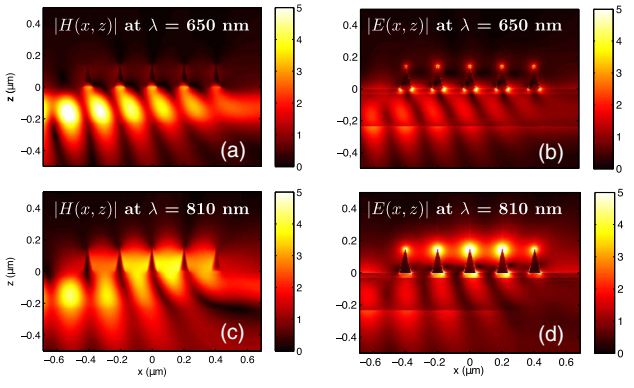

Fig. 7. Distribution of the (a) magnetic and (b) electric fields at $\lambda = 650$ nm. The tip-LSPR is not efficiently excited but rather enhanced at the vertex of the wires due to the simultaneous excitation of the DLM and the oDTM. Distribution of the (c) magnetic and (d) electric fields at $\lambda = 810$ nm. The tip-LSPR is efficiently excited due to the excitation of the eDTM.

4. TOWARD AN INTEGRATED 3D DEVICE: FINITE PERIODIC ARRAY OF GOLD NANOCONES

All the previous results were performed for metallic nanowires of triangular cross section invariant in the out-of-plane direction. In order to compare the tip-LSPR and the optical field enhancement with a three-dimensional structure, namely a finite periodic array of gold nanocones, we performed numerical simulations with the three-dimensional FDTD method (fullwave by RSoft).

The structure consists of a periodic array of five gold nanocones (basis diameter $w = 72$ nm and period $\Lambda = 200$ nm) placed on top of a ridge dielectric waveguide [Fig. 8(a)]. The ridge waveguide has a width $w_{wg} = 500$ nm, a thickness $t_{wg} = 260$ nm, and a core refractive index 2.0, placed on top of the silica substrate. To resemble the burial depth of the two-dimensional case, a silica layer of thickness $t = 30$ nm was placed on top of the dielectric waveguide. The choice of this

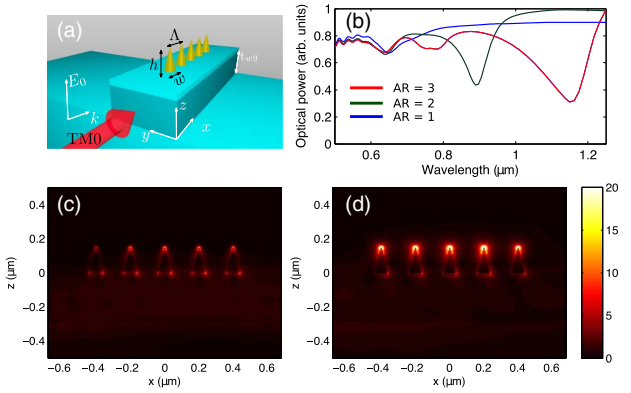

Fig. 8. (a) Schematic of a three-dimensional array of five gold nanocones integrated on top of a ridge dielectric waveguide. (b) Normalized transmission spectra of the integrated system. The excitation of the DTM is observed around $\lambda = \{650, 890, 1150\}$nm for the aspect ratios AR $= \{1, 2, 3\}$, respectively. The reflection curves are almost negligible for the three cases. Near-field maps of the absolute value of the electric field for a three-dimensional periodic array of nanocones placed on top of a ridge waveguide for an AR $= 2$ at (c) $\lambda = 650$ nm and (d) $\lambda = 890$ nm. Like in the two-dimensional case, the excitation of the DLM leads to an enhancement of the electromagnetic field at the lower apexes of the nanocones at $\lambda = 650$ nm and the DTM is efficiently excited at $\lambda = 890$ nm with the TM0 fundamental mode of the dielectric waveguide (AR $= 2$).

ridge waveguide is for practical applications, without changing the physical process for the excitation of the tip-LSPR. Three different aspect ratios (AR = height/width) of the nanocones were simulated, corresponding to heights of 72 nm, 144 nm, and 216 nm. The waveguide is excited with its fundamental TM0 mode.

As can be observed in the transmission spectra of Fig. 8(b), the tip-LSPR is redshifted as the aspect ratio increases. For AR = 1, the tip-LSPR is excited around $\lambda = 650$ nm, for AR = 2 around $\lambda = 890$ nm, and for AR = 3 around $\lambda = 1150$ nm. Also for AR = 2 and AR = 3, there are new resonances observable at shorter wavelengths associated with higher-order modes, as predicted by Tuccio and coauthors [3].

The transmission spectrum for the nanocones of aspect ratio AR = 2, which corresponds to the same aspect ratio of the nanowires with triangular cross section, exhibits two minimum wavelength values around $\lambda = 650$ nm and $\lambda = 890$ nm. The first one is associated with the excitation of a dipolar longitudinal resonance and a contribution of the oDTM [Fig. 8(c)], while the second one corresponds to the excitation of the eDTM. The coupling between the photonic and plasmonic modes, gives rise to a tip-LSPR, having obtained an efficient excitation of the optical field at the top vertices of the nanocones [Fig. 8(d)].

5. CONCLUSIONS

We demonstrated that a tip-LSPR is efficiently excited in a periodic array of triangular-shaped gold nanowires illuminated from the substrate with a TM-polarized plane wave at grazing angles. This tip-LSPR is due to the excitation of a DTM in the nanowires. This mode DTM can be converted into a propagating plasmonic mode if the period of the array is shorter than the wavelength of the incident light (sub-diffractive regime). Even more, a near-field coupling effect between adjacent nanoparticles gives rise to an extraordinary enhancement of the optical electric field at the top vertices of the nanocones. This strong electric field enhancement is a result of the efficient excitation of the electric dipoles oriented along the tip axis of the nanowires. Additionally, we demonstrated the efficient excitation of the plasmonic DTM with the fundamental TM0 photonic mode of a dielectric waveguide placed underneath the subwavelength periodic array of nanowires at visible wavelengths.

The computations done with the periodic and aperiodic Fourier modal method were extended with a three-dimensional simulation performed with the FDTD method to design periodic arrays of gold nanocones integrated on top of a dielectric ridge waveguide. We expect to open new perspectives in the analysis and the design of plasmonic integrated circuits that can be applied in outstanding areas of optics, like lab-on-a-chip nanosensing devices, second-harmonic generation, enhancement of the efficiency of solar cells, or even in the design of new metamaterials.

6. METHODS

To numerically characterize the periodic array of nanowires on top of the silica substrate, we used the FMM, which is a well-known method that solves the Maxwell's equations in the frequency domain. With this method it is possible to directly compute the evanescent and propagative diffracted orders produced by a plane wave illuminating the structure at a given wavelength and angle of incidence, θ_i (Fig. 1). Since this method is formulated for periodic structures, it is only necessary to compute the diffracted orders in a single period of the structure (unitary cell). The triangular cross section of the metallic nanowires within the unitary cell is formed by a stack of lamellar layers (24 layers in our case) parallel to the x direction (stair-case approximation). The relative permittivity of each layer and the incident electromagnetic field are expanded in Fourier series. The insertion of these Fourier series in the Helmholtz equation leads to an eigenvalue problem that can be solved in the frequency domain. The eigenvectors of the eigenvalue problem are associated with the diffracted modes E^{+}_{out} and E^{-}_{out}. These eigenvectors provide the information of the propagation constant; hence the dispersion curves of the modes supported by the structure can also be determined. Also, from the full set of computed diffracted orders, it is then straightforward to determine the transmission, reflection, and absorption spectra normalized to the power of the incident infinite plane wave, as well as the distribution of the local electromagnetic field. A detailed description of the theoretical framework and numerical implementation of the FMM can be found in several references [24,27–34].

Funding. Labex (ANR-11-LABX-01-01); Agence Nationale de la Recherche (ANR) (ANR-12-NANO-0019); Supreme-B (ANR-14-CE26-0015); Conseil Régional Champagne-Ardenne (PLASMOBIO); HPC Center of Champagne-Ardenne ROMEO.

Acknowledgment. The authors thank A. Morand (IMEP-LAHC, Université Joseph Fourier) and P. M. Adam and A. Bruyant (LNIO-ICD, Université de Technologie de Troyes) for having enriched with their comments the content of this work.

REFERENCES

1. K. L. Kelly, E. Coronado, L. L. Zhao, and G. C. Schatz, "The optical properties of metal nanoparticles: the influence of size, shape, and dielectric environment," J. Phys. Chem. B **107**, 668–677 (2003).
2. K. Matsuzaki, S. Vassant, H.-W. Liu, A. Dutschke, B. Hoffmann, X. Chen, S. Christiansen, M. R. Buck, J. A. Hollingsworth, S. Götzinger, and V. Sandoghdar, "Strong plasmonic enhancement of biexciton emission: controlled coupling of a single quantum dot to a gold nanocone antenna," arXiv:1608.07843 (2016).
3. S. Tuccio, L. Razzari, A. Alabastri, A. Toma, C. Liberale, F. D. Angelis, P. Candeloro, G. Das, A. Giugni, E. D. Fabrizio, and R. P. Zaccaria, "Direct determination of the resonance properties of metallic conical nanoantennas," Opt. Lett. **39**, 571–573 (2014).
4. S. D'Agostino, F. Della Sala, and L. C. Andreani, "Dipole-excited surface plasmons in metallic nanoparticles: engineering decay dynamics within the discrete-dipole approximation," Phys. Rev. B **87**, 205413 (2013).
5. C. Noguez, "Surface plasmons on metal nanoparticles: the influence of shape and physical environment," J. Phys. Chem. C **111**, 3806–3819 (2007).
6. C. Schäfer, D. A. Gollmer, A. Horrer, J. Fulmes, A. Weber-Bargioni, S. Cabrini, P. J. Schuck, D. P. Kern, and M. Fleischer, "A single particle plasmon resonance study of 3d conical nanoantennas," Nanoscale **5**, 7861–7866 (2013).
7. A. Horrer, C. Schäfer, K. Broch, D. A. Gollmer, J. Rogalski, J. Fulmes, D. Zhang, A. J. Meixner, F. Schreiber, D. P. Kern, and M. Fleischer,

"Parallel fabrication of plasmonic nanocone sensing arrays," Small **9**, 3987–3992 (2013).
8. C. Schäfer, D. P. Kern, and M. Fleischer, "Capturing molecules with plasmonic nanotips in microfluidic channels by dielectrophoresis," Lab Chip **15**, 1066–1071 (2015).
9. S. Rao, M. J. Huttunen, J. M. Kontio, J. Makitalo, M.-R. Viljanen, J. Simonen, M. Kauranen, and D. Petrov, "Tip-enhanced Raman scattering from bridged nanocones," Opt. Express **18**, 23790–23795 (2010).
10. G. Bautista, M. J. Huttunen, J. Mäkitalo, J. M. Kontio, J. Simonen, and M. Kauranen, "Second-harmonic generation imaging of metal nano-objects with cylindrical vector beams," Nano Lett. **12**, 3207–3212 (2012).
11. G. Bautista, M. J. Huttunen, J. M. Kontio, J. Simonen, and M. Kauranen, "Third- and second-harmonic generation microscopy of individual metal nanocones using cylindrical vector beams," Opt. Express **21**, 21918–21923 (2013).
12. V. Gusak, B. Kasemo, and C. Hägglund, "High aspect ratio plasmonic nanocones for enhanced light absorption in ultrathin amorphous silicon films," J. Phys. Chem. C **118**, 22840–22846 (2014).
13. J.-G. Kim, H. J. Choi, K.-C. Park, R. E. Cohen, G. H. McKinley, and G. Barbastathis, "Multifunctional inverted nanocone arrays for non-wetting, self-cleaning transparent surface with high mechanical robustness," Small **10**, 2487–2494 (2014).
14. J. M. Kontio, H. Husu, J. Simonen, M. J. Huttunen, J. Tommila, M. Pessa, and M. Kauranen, "Nanoimprint fabrication of gold nanocones with 10 nm tips for enhanced optical interactions," Opt. Lett. **34**, 1979–1981 (2009).
15. A. Mustonen, P. Beaud, E. Kirk, T. Feurer, and S. Tsujino, "Efficient light coupling for optically excited high-density metallic nanotip arrays," Sci. Rep. **2**, 915 (2012).
16. O. Saison-Francioso, G. Lévêque, R. Boukherroub, S. Szunerits, and A. Akjouj, "Dependence between the refractive-index sensitivity of metallic nanoparticles and the spectral position of their localized surface plasmon band: a numerical and analytical study," J. Phys. Chem. C **119**, 28551–28559 (2015).
17. H.-N. Wang, A. Dhawan, Y. Du, D. Batchelor, D. N. Leonard, V. Misra, and T. Vo-Dinh, "Molecular sentinel-on-chip for SERS-based biosensing," Phys. Chem. Chem. Phys. **15**, 6008–6015 (2013).
18. M. V. Sosnova, N. L. Dmitruk, A. V. Korovin, S. V. Mamykin, V. I. Mynko, and O. S. Lytvyn, "Local plasmon excitations in one-dimensional array of metal nanowires for sensor applications," Appl. Phys. B **99**, 493–497 (2010).
19. E. D. Palik, *Handbook of Optical Constants of Solids*, 4th ed. (Academic, 1985).
20. J. W. Goodman, *Introduction to Fourier Optics*, 3rd ed. (Roberts & Company, 2005).
21. R. M. A. Azzam, "Circular and near-circular polarization states of evanescent monochromatic light fields in total internal reflection," Appl. Opt. **50**, 6272–6276 (2011).
22. L. Novotny and B. Hecht, *Principles of Nano-Optics*, 2nd ed. (Cambridge University, 2012).
23. L. Józefowski, J. Fiutowski, T. Kawalec, and H.-G. Rubahn, "Direct measurement of the evanescent-wave polarization state," J. Opt. Soc. Am. B **24**, 624–628 (2007).
24. R. Tellez-Limon, M. Fevrier, A. Apuzzo, R. Salas-Montiel, and S. Blaize, "Theoretical analysis of Bloch mode propagation in an integrated chain of gold nanowires," Photonics Res. **2**, 24–30 (2014).
25. D. Maystre, *Theory of Wood's Anomalies*, Springer Series in Optical Sciences (Springer-Verlag, 2012), Vol. **167**.
26. U. Fano, "The theory of anomalous diffraction gratings and of quasi-stationary waves on metallic surfaces (Sommerfeld's waves)," J. Opt. Soc. Am. **31**, 213–222 (1941).
27. P. Lalanne and E. Silberstein, "Fourier-modal methods applied to waveguide computational problems," Opt. Lett. **25**, 1092–1094 (2000).
28. J. P. Hugonin and P. Lalanne, "Perfectly matched layers as nonlinear coordinate transforms: a generalized formalization," J. Opt. Soc. Am. A **22**, 1844–1849 (2005).
29. M. G. Moharam and T. K. Gaylord, "Rigorous coupled-wave analysis of planar-grating diffraction," J. Opt. Soc. Am. **71**, 811–818 (1981).
30. P. Lalanne and G. M. Morris, "Highly improved convergence of the coupled-wave method for TM polarization," J. Opt. Soc. Am. A **13**, 779–784 (1996).
31. L. Li, "New formulation of the Fourier modal method for crossed surface-relief gratings," J. Opt. Soc. Am. A **14**, 2758–2767 (1997).
32. G. Granet and J.-P. Plumey, "Parametric formulation of the Fourier modal method for crossed surface-relief gratings," J. Opt. A **4**, S145–S149 (2002).
33. N. M. Lyndin, O. Parriaux, and A. V. Tishchenko, "Modal analysis and suppression of the Fourier modal method instabilities in highly conductive gratings," J. Opt. Soc. Am. A **24**, 3781–3788 (2007).
34. D. Bucci, B. Martin, and A. Morand, "Application of the three-dimensional aperiodic Fourier modal method using arc elements in curvilinear coordinates," J. Opt. Soc. Am. A **29**, 367–373 (2012).